THE JOURNAL OF BIOLOGICAL CHEMISTRY VOL. 288, NO. 16, pp. 11191–11202, April 19, 2013

Notch Transcriptional Control of Vascular Smooth Muscle Regulatory Gene Expression and Function*[S]

Received for publication, December 6, 2012, and in revised form, March 11, 2013 Published, JBC Papers in Press, March 12, 2013, DOI 10.1074/jbc.M112.442996

Sanchita Basu[1], Dinesh Kumar Srinivasan[1,2], Ke Yang, Hema Raina[3], Suhanti Banerjee, Rongli Zhang, Steven A. Fisher[3], and Aaron Proweller[4]

From the Department of Medicine, Case Cardiovascular Research Institute, and University Hospitals Harrington Heart and Vascular Institute, Case Western Reserve University, Cleveland, Ohio 44106

Background: Notch signaling in smooth muscle is necessary for arterial maturation.
Results: In mice and vessels, Notch signaling deficiency reduces MLCK and phosphorylated MLC content concomitantly with blunted pressor responses and attenuated agonist-induced vasoreactivity.
Conclusion: Smooth muscle *MLCK* is transcriptionally controlled by Notch signaling.
Significance: Functional regulation of smooth muscle contractility by Notch signaling offers novel insights and strategies for modulating systemic arterial reactivity.

Notch receptors and ligands mediate heterotypic cell signaling that is required for normal vascular development. Dysregulation of select Notch receptors in mouse vascular smooth muscle (VSM) and in genetic human syndromes causes functional impairment in some regional circulations, the mechanistic basis of which is undefined. In this study, we used a dominant-negative Mastermind-like (DNMAML1) to block signaling through all Notch receptors specifically in VSM to more broadly test a functional role for this pathway *in vivo*. Mutant DNMAML1-expressing mice exhibited blunted blood pressure responses to vasoconstrictors, and their aortic, femoral, and mesenteric arteries had reduced contractile responses to agonists and depolarization *in vitro*. The mutant arteries had significant and specific reduction in the expression and activity of myosin light chain kinase (MLCK), a primary regulator of VSM force production. Conversely, activated Notch signaling in VSM cells induced endogenous *MLCK* transcript levels. We identified *MLCK* as a direct target of activated Notch receptor as demonstrated by an evolutionarily conserved Notch-responsive element within the *MLCK* promoter that binds the Notch receptor complex and is required for transcriptional activity. We conclude that Notch signaling through the transcriptional control of key regulatory proteins is required for contractile responses of mature VSM. Genetic or pharmacological manipulation of Notch signaling is a potential strategy for modulating arterial function in human disease.

The Notch signaling cascade provides critical functions during vertebrate vascular development and postnatal maturation. Notch receptors (Notch1–4) are single pass transmembrane proteins activated by interactions with ligands (Delta and Jagged) present on neighboring cell membranes, resulting in a γ-secretase-dependent receptor cleavage and translocation of the Notch intracellular domain into the nucleus. In canonical Notch signaling, Notch intracellular domain partners with the transcriptional activator Mastermind and a DNA-binding protein, CBF1/Su(H)/Lag2 protein (CSL[5]; also known as RBP-Jκ), targeting the complex to gene promoters containing the consensus motif GTGGGAA (1–3). In vascular wall cells, *HRT*/*HEY* basic helix-loop-helix genes have been identified as important targets and functional mediators of Notch receptor activation, particularly during developmental angiogenesis and postnatal vascular injury responses (4, 5).

In humans, mutations in the Notch3 receptor are linked to cerebral autosomal dominant arteriopathy with subcortical infarcts and leukoencephalopathy (CADASIL) syndrome, which features a progressive non-atheromatous arteriopathy in brain arterioles punctuated by vessel stenoses, cerebral ischemia, and infarction (6). Modeling of this syndrome and that of deletion of the Notch3 receptor in mice further uncovered impaired myogenic responses in caudal, cerebral, and renal arteries (7–11). Investigations in these animals revealed altered contractile gene content as well as reduced levels of phosphorylated myosin light chain (MLC) attributed to defective RhoA/Rho kinase signaling (7, 8). However, vascular dysfunction was

* This work was supported, in whole or in part, by National Institutes of Health Grants HL096603 (to A. P.) and HL066171 (to S. F.).
[S] This article contains supplemental Figs. 1 and 2.
[1] Both authors contributed equally to this work.
[2] Present address: Lee Kong Chian School of Medicine, Nanyang Technological University, Singapore 637553, Singapore.
[3] Present address: Dept. of Medicine, Division of Cardiology, University of Maryland, Baltimore, MD 21201.
[4] To whom correspondence should be addressed: Dept. of Medicine, Case Western Reserve University, 4530 Wolstein Research Bldg., 2103 Cornell Rd., Cleveland, OH 44122. Tel.: 216-368-0131; Fax: 216-368-0556; E-mail: aaron.proweller@case.edu.

[5] The abbreviations used are: CSL, CBF1/Su(H)/Lag2 protein; VSM, vascular smooth muscle; DNMAML1, dominant-negative Mastermind-like; MLCK, myosin light chain kinase; CADASIL, cerebral autosomal dominant arteriopathy with subcortical infarcts and leukoencephalopathy; MLC, myosin light chain; MP, myosin phosphatase; p-MLC, phosphorylated MLC; SMC, smooth muscle cell; IC, internal circumference; FA, femoral artery; TA, thoracic aorta; MA, mesenteric artery; PE, phenylephrine; ACh, acetylcholine; SNP, sodium nitroprusside; HR, high relaxing; Ang II, angiotensin II; MAP, mean arterial blood pressure; DAPT, *N*-[*N*-(3,5-difluorophenacetyl-L-alanyl)]-*S*-phenylglycine *t*-butyl ester; SM-MHC, smooth muscle myosin heavy chain; αSMA, *α-smooth muscle actin;* ICN1, intracellular Notch1; CC, core CSL; CArG, CC[A/T]6GG; HRT, Hairy-related transcription-factor.

not detected in most systemic arterial and resistance vasculature, suggesting a regional and complex influence through which impaired Notch3 signaling affected vascular smooth muscle myogenic responses. Importantly, smooth muscle Notch signaling was not abolished in these animal models due to expression of additional Notch receptors and pathway components.

Force of contraction of VSM is determined by the opposing activities of MLCK and myosin phosphatase (MP), and MLCK is required for both physiological and pathological blood pressure (12, 13). MLCK expression is transcriptionally regulated by serum response factor and its co-activator, myocardin (14, 15). Functionally, Ca^{2+}/calmodulin-dependent MLCK activity phosphorylates MLC (p-MLC) and activates the myosin ATPase, causing contraction, whereas phosphate removal by MP inactivates myosin, causing relaxation (16, 17).

Given the unique vascular myogenic deficits associated with dysregulation of a single Notch receptor (Notch3), the current study was designed to more broadly examine vascular function and identify critical targets of Notch signaling by disrupting the canonical pathway in VSM. We hypothesized that Notch signals modulate the transcription of key regulatory contractile proteins and tested this by examining expression and function in a mouse model expressing a dominant-negative Mastermind-like (DNMAML1) protein to inhibit (CSL-dependent) Notch signaling targeted specifically to smooth muscle with the SM22α-Cre promoter (18). This model suppresses canonical signaling through all Notch receptors, therefore overcoming potential functional redundancies and providing a more comprehensive assessment of Notch signaling contribution in VSM. Through this approach, we have identified a novel role for Notch signaling in the regulation of arterial contractile function through transcriptional control of smooth muscle MLCK.

EXPERIMENTAL PROCEDURES

Animals—Animal care and experimental procedures were conducted in accordance with the National Institutes of Health's Guide for the Care and Use of Laboratory Animals and approved and monitored by the Case Western Reserve University Institutional Animal Care and Use Committee. The generation and initial characterization of SM22-Cre^+/$DNMAML1^+$ (DNMAML1-expressing) mutant and SM22-Cre^-/$DNMAML1^+$ (non-DNMAML1-expressing) littermate control mice were reported previously, including the demonstrated suppression of induced Notch signaling activity in DNMAML-expressing aortic smooth muscle cells (18). All mice, including the parental SM22-Cre^+ and conditional DNMAML1 lines, were maintained on a C57Bl/6 genetic background.

Cell Culture and Transfections—C3H10T1/2 (10T1/2) myofibroblasts and A10 rat aortic smooth muscle cells (ATCC) were maintained in Dulbecco's modified Eagle's medium (Invitrogen) supplemented with 10% fetal bovine serum (HyClone). Transient plasmid transfections were performed using Xtremegene transfection reagent (Roche Applied Science) with a 3:1 Xtremegene/DNA ratio, and cells were collected after 48 h. Cultured primary aortic SMCs from control and mutant mice were isolated and propagated as described previously (18). Where indicated, cultured aortic SMCs were depolarized with 60 mM KCl for up to 30 min.

Isometric Tension Measurement—Adult mice (10–12 weeks old) were euthanized by CO_2 inhalation. Segments of thoracic aorta (TA), femoral artery (FA), and mesenteric artery (MA) were dissected, cut into 2–3-mm rings, and suspended in an isometric tension myograph (Model 610M, Danish Myo Technology, Aarhus, Denmark) chamber containing PSS buffer (112.0 mM NaCl, 25.7 mM $NaHCO_3$, 4.9 mM KCl, 2.0 mM $CaCl_2$, 1.2 mM $MgSO_4$, 1.2 mM KH_2PO_4, 11.5 mM glucose, and 10.0 mM Hepes (pH 7.4) equilibrated with a gas mixture of 95% O_2 and 5% CO_2 at 37 °C as described previously (19). All chemicals were purchased from Sigma unless otherwise specified. The resting tension-internal circumference (IC) relation was determined for each FA and MA segment (20). IC was set to 0.9 Å ~ IC_{100} where IC_{100} is the internal circumference of the vessel under an effective transmural pressure of 100 mm Hg (13.3 kilopascals). For TA rings, base-line tension in PSS buffer was preset at 4 millinewtons prior to force induction. Cumulative dose-response curves to phenylephrine (PE; an α-adrenergic receptor agonist; 1 nM to 10 μM), acetylcholine (ACh; muscarinic receptor agonist; 10 nM to 10 μM), and sodium nitroprusside (SNP; direct NO donor; 10 nM to 10 μM) were generated in the absence or presence of 100 μM L-nitroarginine methyl ester (competitive antagonist of L-arginine/NO production). Dose-response curves were performed with single agents and repeated in triplicate at each concentration. For depolarization-induced contractility studies, 60 mM KCl was added to the reaction bath after vessel equilibration in PSS buffer. Treatment regimens are described in each figure legend. Data are presented as active tension (millinewtons) for agonist-induced contraction and percentage of maximum PE-induced tension for ACh- and SNP-mediated relaxation.

Calcium Permeabilization and Force Generation Studies—Arteries were permeabilized, and force-calcium relationships were determined as described previously with minor modifications (21). In brief, isolated TA and MA segments were mounted in the wire myograph and incubated in high relaxing (HR) solution for 10–20 min and permeabilized with 1000 units/ml α-toxin (Calbiochem) in HR solution for 1 h at room temperature. The HR solution (pCa >9) was composed of 53.28 mM KCl, 6.81 mM $MgCl_2$, 0.025 mM $CaCl_2$, 10.0 mM EGTA, 5.4 mM Na_2ATP, and 12.0 mM creatine phosphate. After permeabilization, segments were washed with additional HR solution. HR and pCa solutions used during and following permeabilization of the arteries were designed (MAXC computer program) to maintain a desired free Ca^{2+} concentration using Ca^{2+}-EGTA buffering. The composition of the pCa 4.5 solution was similar to HR solution except for the following differences: 33.74 mM KCl, 6.48 mM $MgCl_2$, and 9.96 mM $CaCl_2$. The pH of the HR and pCa 4.5 solutions was adjusted to 7.1 with KOH, and ionic strength was held constant (0.15). Solutions containing a desired free Ca^{2+} concentration between pCa 9 and 4.5 were achieved by mixing appropriate volumes of HR and pCa 4.5 solutions based on the Bathe algorithm. All solutions contained the protease inhibitors leupeptin (1 μg/ml), pepstatin A (2.5 μg/ml), and PMSF (50 μM). The pCa-tension relationship was then determined by bathing the permeabilized vessels in solu-

tions of sequentially increasing Ca^{2+} concentrations, ranging from *p*Ca 8.5 to 4.5, while recording active tension for ~5 min in each solution or until stabilized.

Blood Pressure Measurements—Adult mice (8–12 weeks old) were anesthetized with tribromoethanol (Avertin; 0.25 mg/g of body weight intraperitoneally) and secured in the supine position. The right internal jugular vein was surgically exposed and cannulated for drug infusions. Following calibration, a 1F pressure catheter (SPR-1000, Millar Instruments) was inserted into the left common carotid artery and advanced toward the heart until a stable aortic pressure waveform was observed (PowerLab data acquisition unit, ADInstruments). Heart rates were simultaneously measured through needle electrodes and bioamplification under a separate channel. Animals received escalating doses of either PE (5, 20, and 100 μg/kg) or angiotensin II (Ang II) (0.05, 0.5, and 5 μg/kg). Each bolus injection delivered a total volume of 30 μl (adjusted to effective concentration) and was performed in triplicate with return to base-line blood pressure prior to each injection. Hemodynamic data analyses were performed using LabChart software (ADInstruments). Data are displayed as absolute change from base line in mean arterial blood pressure (MAP; in mm Hg). MAP was calculated as the sum of the area under the aortic pressure curve averaged over a minimum 100 cardiac cycles. Where indicated, mice were administered *N*-[*N*-(3,5-difluorophenacetyl-L-alanyl)]-*S*-phenylglycine *t*-butyl ester (DAPT; 10 mg/kg subcutaneously; Calbiochem) or vehicle (DMSO) daily for 6 days followed by PE dose-response measurements.

Cardiac Function Analyses—Mice (8–12 weeks old) were anesthetized with Avertin (0.25 mg/g of body weight intraperitoneally), and transthoracic echocardiography was performed using the Vevo 770 High Resolution Imaging System (Visual Sonics, Canada) equipped with an RMV-707B 30-MHz probe. Standard M-mode sampling was taken through the left ventricular short axis at the midpapillary level before and 1 min after PE treatment via tail vein injection. A 30-μl bolus volume was maintained for each PE dose.

Immunohistochemistry—Tissues were fixed with 4% paraformaldehyde in PBS at 4 °C overnight and cryoprotected with 15% sucrose. Transverse sections (10 mm) were cut using a cryostat (Leica CM3050), washed with PBS, and blocked in 1% BSA for 1 h at room temperature. Serial sections were incubated at 4 °C overnight with primary antibodies against smooth muscle myosin heavy chain (SM-MHC) (1:100; Abcam), αSMA (1:100; Sigma), cleaved Notch1 (1:100; Cell Signaling Technology), or Jagged1 (1:100; Santa Cruz Biotechnology) in PBS containing 0.1% Triton X-100 (PBS-TX). Sections were washed in PBS and incubated with anti-rabbit IgG conjugated to DyLight 594 (1:200; Jackson ImmunoResearch Laboratories, West Grove, PA) or anti-mouse IgG conjugated to Cy3 (1:200; Sigma) diluted in PBS-TX for 1 h at room temperature. Sections incubated as described above but without the primary antibodies served as negative controls. Sections were mounted with DAPI (Dako) and viewed, and images were captured by high resolution fluorescence microscopy.

Western Blotting—Arterial segments were quickly dissected, snap frozen in liquid nitrogen, and homogenized in radioimmune precipitation assay buffer (50 mM Tris-Cl (pH 7.4), 150 mM NaCl, 1% Nonidet P-40, 0.25% sodium deoxycholate, and 1 mM PMSF) containing protease inhibitors (Roche Applied Science) and phosphatase inhibitor (Pierce). Alternatively, primary aortic SMCs from control and mutant mice were isolated, and total protein lysates were collected as described previously (22). Protein concentrations were determined by Bradford assay (Bio-Rad). Western blotting was performed as described previously (23). Briefly, proteins were transferred to nitrocellulose membranes by standard semidry methods (Bio-Rad). The membranes were incubated for 1 h at room temperature with blocking buffer and then with antibodies against MLCK (mouse monoclonal; Sigma; 1:10,000), MLC (rabbit polyclonal; Cell Signaling Technology; 1: 1000), p-MLC (rabbit polyclonal; Cell Signaling Technology; 1:1,000 (24)), αSMA (mouse monoclonal; Sigma; 1:200), SM-MHC (rabbit polyclonal; Abcam; 1:1,000), cleaved Notch1 (rabbit polyclonal; Cell Signaling Technology; 1:1000), or β-actin (rabbit polyclonal; Sigma; 1:1,000) in blocking solution overnight at 4 °C. Thereafter, secondary antibodies included horseradish peroxidase (HRP)-conjugated anti-mouse IgG for MLCK and αSMA (Cell Signaling Technology; 1:5,000) and HRP-conjugated anti-rabbit IgG for MLC, p-MLC, SM-MHC, cleaved Notch1, and β-actin (Cell Signaling Technology; 1:10,000). Proteins were detected by enhanced chemiluminescence according to the manufacturer's instructions (Cell Signaling Technology), and films were digitally scanned for protein quantification using NIH Image software. Relative densitometric units for MLCK, SM-MHC, and αSMA were calculated by normalization to β-actin, whereas p-MLC was normalized to total MLC.

Depolarization and Agonist Treatment of Isolated Aortic Ring Explants—Thoracic aortas were quickly harvested from mutant and littermate control mice and segmented into 4-mm-long rings, each equilibrated in PSS buffer containing protease (Sigma) and phosphatase inhibitors (Roche Applied Science) at 37 °C. Thereafter, rings were treated with either 60 mM KCl or 10^{-5} M Ang II for 15 min and immediately transferred to a fresh PSS buffer wash, and snap frozen in liquid nitrogen. Frozen segments were homogenized in radioimmune precipitation assay lysis buffer using TissueLyser II (2 × 2 min at 30 Hz; Qiagen). Lysates were centrifuged at 10,000 × *g* for 10 min at 4 °C, and the supernatants were collected for Western blot detection of phosphorylated and total MLC as described above.

Real Time PCR (Quantitative PCR) Analysis of MLCK mRNA—From whole tissue, arterial segments were quickly dissected, snap frozen in liquid nitrogen, and homogenized in TRIzol reagent (Invitrogen) followed by standard RNA extraction. Total RNA was also isolated from A10 and primary aortic SMCs collected in TRIzol. Two micrograms of total RNA served as template for oligo(dT)-primed reverse transcription using SuperScript III reverse transcriptase (Invitrogen). Real time PCR analyses were performed on a StepOnePlus quantitative PCR system (Applied Biosystems) using mouse *MLCK* primers reported previously (25). *MLCK* primers for A10-derived transcripts included 5′-GACGTGTTCACCCTGGTTCT-3′ (forward) and 5′-TTTGTGCAGCATCAGTGACA-3′ (reverse). Primers for *HRT1* and *HRT2* have been described previously (26). The PCR included 50 ng of cDNA reaction, 150 nM for-

ward and reverse *MLCK* primers, and 1× SYBR Green (Applied Biosystems). *GAPDH* amplification served as the reference gene. Reactions were performed in triplicate, and data were analyzed according to the $2^{-\Delta\Delta c(t)}$ method.

Luciferase Reporter Studies and Site-directed Mutagenesis—Luciferase reporter assays were performed in 10T1/2 cells (ATCC) as described previously (26). Briefly, cells were seeded in 24-well tissue culture plates and co-transfected using Xtremegene transfection reagent (Roche Applied Science) with 25 ng of p6476 or p389 *MLCK*-luciferase reporter constructs (a kind gift from Dr. Paul Herring, Indiana University) and expression plasmids for intracellular Notch1 (ICN1) and DNMAML1 at the indicated ratios (15, 26). As described previously (15), plasmid p6476 contains nucleotides −6476 through +115 of the *MLCK* promoter, and p389 is a truncated promoter containing nucleotides −389 through +115 (see Fig. 7*A*, schematic). Both p6476 and p389 contain a CArG element required for serum response factor/myocardin-induced transcription, and therefore inclusion of a myocardin expression plasmid in these experiments served as a positive control for activation of the promoter/reporter (26). Cells were harvested 48 h after plasmid transfection for measurement of luciferase activity (Promega) using a Veritas plate reader (Turner BioSystems) and normalized to total protein. Experiments were repeated in triplicate. For promoter mutagenesis studies, p6476 was used as the template for a single nucleotide substitution at a core CSL (CC) sequence located at position −3685 (G to A). Mutagenesis primers included 5′-GGAATGAGGGACCTGAGAATTCATGCTGGTC-3′ (2FCSLf) and 5′-GACCAGCATGAATTCTCAGGTCCCTCATTCC-3′ (2FCSLr), and the procedure was performed using a QuikChange II site-directed mutagenesis kit (Agilent Technologies) according to the manufacturer's instruction. Two independent mutant clones (p2FCSL2 and p2FCSL5) were confirmed by DNA sequencing and subjected to luciferase assay as above.

Notch Ligand Stimulation Assay—Notch signaling was induced in control SM22-Cre$^-$/DNMAML1$^+$ aortic SMCs cultured in dishes displaying immobilized Jagged1 ligand (Fc-Jag1) as described previously (26).

Chromatin Immunoprecipitation (ChIP)—Experiments were performed according to the ChIP assay kit protocol (Millipore). Briefly, following indicated plasmid transfection (for 10T1/2 or A10) or Fc-Jag1 treatment (for primary aortic SMCs), cells were fixed by addition of formaldehyde (1%) to the culture medium for 10 min at 37 °C, washed in PBS, scraped, and resuspended in lysis buffer for 10 min at 4 °C. DNA was sheared to ~500-bp fragments using a Bioruptor apparatus. A fixed volume of lysate was removed as DNA input control, and the remaining suspension was diluted 10-fold with dilution buffer and further precleared with protein A-agarose/salmon sperm DNA slurry. Recovered supernatants were incubated with 2 μg of Notch1 antibody (sc-6014, Santa Cruz Biotechnology) or rabbit IgG overnight at 4 °C. Immunoprecipitated complexes were collected by pulldown with protein A-agarose/salmon sperm DNA. The precipitates were extensively washed and incubated in elution buffer. Cross-linking of protein-DNA complexes was reversed, and DNA was recovered by phenol/chloroform extraction and ethanol precipitation. Both input and immunoprecipitated DNAs were subjected to PCR using primers 5′-TTTGACCTCCATCAGATGGTC-3′ (forward) and 5′-AACTTTCCACTGACTTGCTCC-3′ (reverse) encompassing the putative −3687 CSL binding site in the *MLCK* promoter.

TABLE 1
Base-line animal weight, MAP, and heart rate (HR) indices in Notch signaling-deficient (Cre$^+$) and control (Cre$^-$) mice
Data represent mean ± S.E.; $n = 5$ per cohort. Cre$^+$, SM22-Cre$^+$/DNMAML1$^+$; Cre$^-$, SM22-Cre$^-$/DNMAML1$^+$; bpm, beats/min.

	Cre$^-$	Cre$^+$	*p* value
Body weight (g)	20.2 ± 1.6	19.2 ± 2.1	0.10
Heart rate (bpm)	469 ± 49	514 ± 80	0.49
Mean arterial blood pressure (mm Hg)	95 ± 9	91 ± 9	0.20

Statistical Analysis—All data are presented as mean ± S.E. Significance of differences between groups was determined by analysis of variance or by Student's *t* test. A probability value of <0.05 was considered statistically significant.

RESULTS

SM22-Cre$^+$/DNMAML1$^+$ Mice Exhibit Blunted Pressor Responses to Vasoconstrictors—Anesthetized control and Notch signaling-deficient (SM22-Cre$^+$/DNMAML1$^+$) mice were subjected to continuous intra-arterial blood pressure recording while being exposed to escalating concentrations of vasoconstrictors. Base-line heart rate and blood pressure were similar between cohorts (Table 1). However, in mutant mice, the pressor response to bolus intravascular injection of PE or Ang II was blunted at all concentrations tested and achieved only 55 and 67% of control increment at maximal doses of PE (100 μg/kg) and Ang II (5 μg/kg), respectively (Fig. 1, *A* and *B*). Expression of the SM22-Cre recombinase alone did not influence blood pressure responses (Fig. 1*C*). We also assessed pressor responses in control mice pretreated with the non-tissue-specific pharmacological Notch signaling inhibitor DAPT and determined a significantly blunted blood pressure response with maximal PE (100 μg/kg) (Fig. 1*D*). Finally, we interrogated cardiac performance by transthoracic echocardiography, revealing similar functional indices between cohorts both at base line and with PE treatment (Table 2). Therefore, inhibition of canonical Notch signaling either through elaboration of DNMAML1 or by DAPT suggested the possibility of intrinsic deficiencies in vascular smooth muscle contractile capacity.

Inhibition of VSM Notch Signaling Impairs Arterial Vessel Contractile Function—To determine whether the blunted pressor responses observed in mutant mice reflect altered vascular function, we investigated contractile function of arteries derived from SM22-Cre$^+$/DNMAML1$^+$ and littermate control mice using wire myography. Mutant TA and FA rings produced significantly less force in response to the α-agonist PE (Fig. 2, *A* and *D*, respectively). This difference in force production remained when rings were pretreated with L-nitroarginine methyl ester (100 μM) to block nitric-oxide synthesis (Fig. 2, *B* and *E*). The dose response of the mutant arteries to a second contractile agonist, Ang II, was also significantly decreased although not to the same magnitude (Fig. 2, *C* and *F*). We next examined contractile function in a representative resistance

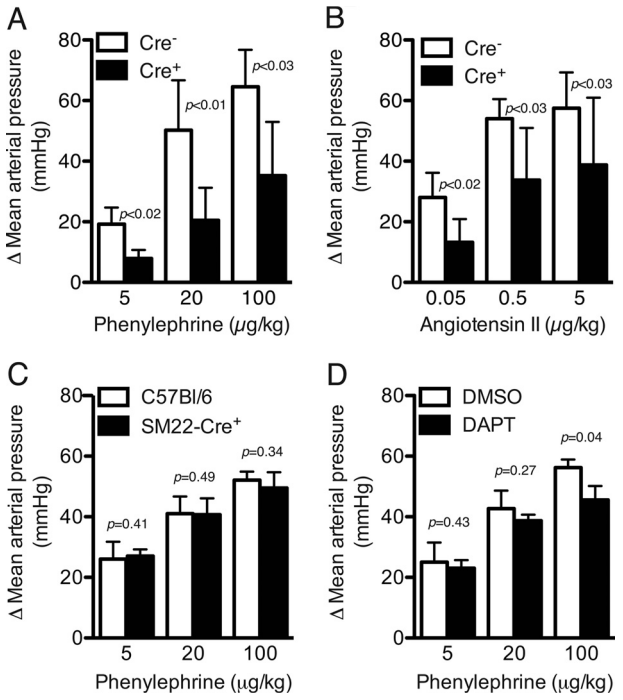

FIGURE 1. **Agonist-induced blood pressure response is significantly blunted in Notch signaling-deficient animals.** Control SM22-Cre$^-$/DNMAML1$^+$ (*Cre*$^-$) and SM22-Cre$^+$/DNMAML1$^+$ (*Cre*$^+$) mice received intravenous bolus infusions of either PE (*A*) or Ang II (*B*) in escalating doses. Induced arterial vasoconstriction from either agonist yielded significantly less MAP change (mm Hg) in SM22-Cre$^+$/DNMAML1$^+$ animals. Data are displayed as change in MAP relative to base-line pressure. Data sets represent mean ± S.E. (*error bars*); $n = 5$ per cohort. *C*, PE dose-response curve in parental SM22-Cre$^+$ transgenic *versus* C57Bl/6 animals. Cre recombinase expression alone does not affect agonist-induced blood pressure responses. Data are displayed as change in MAP relative to base-line blood pressure (C57Bl/6, 82 ± 4.1 mm Hg *versus* SM22-Cre$^+$, 81 ± 1.4 mm Hg; p = not significant). Data represent mean ± S.E. (*error bars*); $n = 5$ per cohort. *D*, DAPT treatment results in blunted blood pressure responses with high dose PE. Control mice were pretreated with DAPT or vehicle (DMSO) followed by PE dose response. Data are displayed as change in MAP relative to base-line blood pressure (DMSO, 92 ± 4.4 mm Hg *versus* DAPT, 94 ± 3.8 mm Hg; p = not significant). Data represent mean ± S.E. (*error bars*); $n = 5$ per cohort.

TABLE 2

Echocardiographic parameters in Notch signaling-deficient (Cre$^+$) and control (Cre$^-$) mice

Standard M-mode measurements were obtained at base line and following acute intravenous infusion of PE. Data represent mean ± S.E.; $n = 6$ per cohort. Cre$^+$, SM22-Cre$^+$/DNMAML1$^+$; Cre$^-$, SM22-Cre$^-$/DNMAML1$^+$; wt, body weight; HR, heart rate; IVS(d), interventricular septum (diastole); IVS(s), interventricular septum (systole); LVPW(d), left ventricular posterior wall (diastole); LVPW(s), left ventricular posterior wall (systole); FS, fractional shortening; EF, ejection fraction; bpm, beats/min.

	Cre$^-$	Cre$^+$	p value
Base line			
wt (g)	19.02 ± 0.74	18.27 ± 0.75	0.49
HR (bpm)	546.8 ± 8.51	535.8 ± 19.48	0.62
IVS(d) (mm)	0.63 ± 0.01	0.66 ± 0.03	0.39
IVS(s) (mm)	1.00 ± 0.03	0.94 ± 0.04	0.34
LVPW(d) (mm)	0.69 ± 0.03	0.76 ± 0.05	0.31
LVPW(s) (mm)	1.06 ± 0.05	1.13 ± 0.05	0.39
FS (%)	36.63 ± 1.39	34.10 ± 1.48	0.24
EF (%)	67.24 ± 1.81	64.12 ± 2.03	0.28
PE (100 μg/kg)			
HR (bpm)	557.8 ± 5.55	556.5 ± 16.66	0.95
IVS(d) (mm)	0.67 ± 0.03	0.73 ± 0.04	0.26
IVS(s) (mm)	0.99 ± 0.04	1.03 ± 0.04	0.46
LVPW(d) (mm)	0.81 ± 0.05	0.80 ± 0.07	0.89
LVPW(s) (mm)	1.20 ± 0.07	1.18 ± 0.08	0.86
FS (%)	37.33 ± 1.87	37.43 ± 1.70	0.97
EF (%)	67.94 ± 2.43	68.28 ± 2.16	0.92

vessel, the third-order MA, more relevant to the control of blood pressure as compared with the larger arteries studied above. The mutant MA rings produced significantly less force in response to PE at the highest concentration (10^{-5} M) of the dose-response curve (Fig. 2*G*).

To determine whether the defect in agonist-induced force production of the mutant arteries may be due to an intrinsic defect in the VSM, vessels were activated by KCl (60 mM)-induced depolarization. Mutant TA, FA, and MA rings achieved only 38, 20, and 65%, respectively, of the force of control arterial rings (Fig. 3*A*). To determine whether the defect in force production of the mutant arteries resided at the level of the myofilaments, vessels were permeabilized, and calcium-force relationships were determined. Both mutant TA and MA produced less force at maximal (pCa 4.5) and submaximal (pCa 5.5) calcium concentrations as compared with the control arteries (Fig. 3*B*). Thus, Notch signaling deficiency in VSM causes a defect in contractile responses to agonists and depolarization that at least in part results from reduced calcium activation of force production by the myofilaments.

Inhibition of VSM Notch Signaling Impairs Arterial Relaxation—To determine whether the defect in VSM force production was accompanied by impairment in relaxation, arterial rings were treated with ACh (an endothelium-dependent vasorelaxant) or SNP (an endothelium-independent vasorelaxant). Vascular rings were precontracted with submaximal (10^{-5} M) PE followed by dose-response studies of ACh and SNP. Compared with control rings, both mutant FA and MA vessels exhibited significantly reduced relaxation responses to either ACh or SNP (Fig. 4). This differential response was more pronounced in the MA, including at the highest dose (10^{-5} M) of ACh and SNP (Fig. 4, *B* and *D*). Thus, Notch signaling deficiency in VSM causes a defect in relaxant responses to a direct vasodilator, again implicating a defect in regulation of force production at the level of the myofilaments.

Notch Signaling-deficient Vessels and Aortic Smooth Muscle Cells Exhibit Dysregulation of Select Contractile Proteins—The reduced calcium sensitivity of force production and reduced sensitivity to contractile agonists and antagonists suggested altered expression or activity of contractile regulatory proteins. Indeed, MLCK, the principle kinase responsible for penultimate MLC phosphorylation, was reduced to 38% of control in mutant aorta, and the level of p-MLC was likewise reduced to 34% of control (Fig. 5, *A* and *B*). Notably, total MLC content was unchanged, resulting in a mutant ratio of p-MLC to total MLC of 52% of control (Fig. 5*B*, *box inset*). Moreover, KCl or Ang II treatment markedly induced p-MLC in control but not mutant aortic ring explants despite similar total MLC content (Fig. 5*C*). Finally, depolarization of cultured mutant aortic SMCs with 60 mM KCl for up to 30 min failed to elicit MLC phosphorylation in contrast to control cells (Fig. 5*D*), whereas MLCK protein and transcript levels were unaffected by KCl (data not shown). These studies highlight inefficient production of p-MLC in mutant arterial smooth muscle consistent with reduced MLCK content.

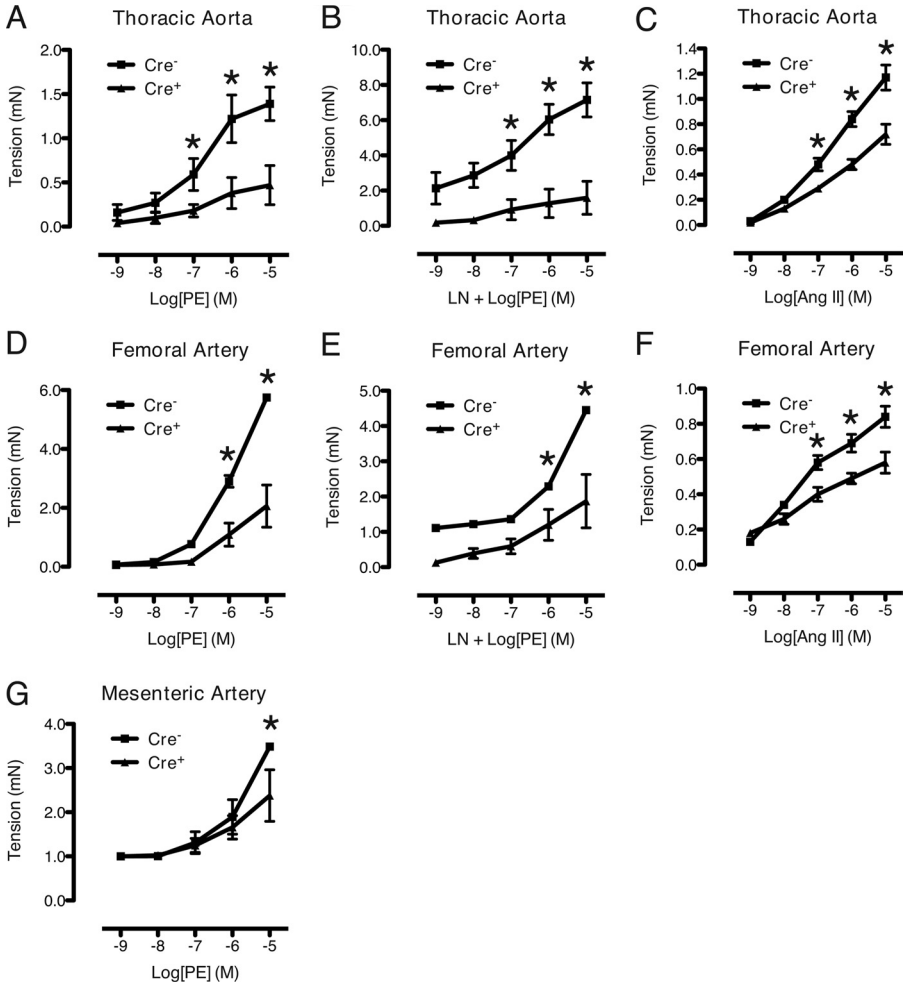

FIGURE 2. **Inhibition of Notch signaling in VSM impairs agonist-induced contractility.** *A*, *B*, *D*, *E*, and *G*, dose-response curves for PE-treated vessels. PE was applied to control (*Cre*$^{-}$) and mutant (*Cre*$^{+}$) segments of thoracic aorta (*A*), femoral artery (*D*), and mesenteric artery (*G*). L-Nitroarginine methyl ester (*LN*) pretreatment was included in *B* and *E*, respectively. *C* and *F*, dose-response curves for Ang II-treated thoracic aorta and femoral arteries, respectively. Generated tension was consistently reduced in mutant vessels. Data are displayed as active tension relative to base line (PSS buffer only). Measurements were repeated in triplicate at each dose. Each data set represents mean ± S.E. (*error bars*); $n = 3$ control and 3 mutant. *, $p < 0.02$ *versus* control. *mN*, millinewtons.

Notably, immunohistochemical staining and Western blot analyses revealed similar αSMA and SM-MHC expression patterns and content in the tunica media in control and mutant aortas and derived SMCs (Fig. 6), and there were no differences in cross-sectional area between control and mutant vessels or in the numbers and thickness of VSM layers within the aortic tunica media (Fig. 6, *A–D*, *white boxes*, and data not shown). Taken together, these data suggest that Notch signals control the expression and/or activity of key regulatory proteins that control force production in smooth muscle without affecting myofilament content.

MLCK Transcript Levels and Promoter Are Sensitive to Canonical Notch Signaling—The reduced levels of MLCK protein in Notch signaling-deficient aortas and derived aortic SMCs prompted an inspection of *MLCK* gene expression. Analyses of RNA collected from mutant aortas and smooth muscle cells revealed parallel reductions in *MLCK* transcripts (Fig. 5*E*). Conversely, we measured endogenous *MLCK* gene expression in Notch signaling-activated SMCs. First, control primary aortic SMCs were seeded on plates displaying fixed Jagged1 ligand (extracellular domain) to further stimulate Notch receptors, resulting in an ~6-fold increase in *MLCK* transcripts (Fig. 5*F*, *upper left*). To confirm signaling activation in this assay, we observed the expected induction of the known Notch target gene *HRT2* (Fig. 5*F*, *lower left*). Notably, this method of induced Notch signaling is particularly relevant because Jagged1 and activated Notch receptor are present in the smooth muscle tunica media of intact aorta (supplemental Fig. 1). Second, forced expression of constitutively active Notch1 (ICN1) in the rat A10 aortic SMC line also resulted in a severalfold increase in endogenous *MLCK* transcripts along with a predictable rise in expression of the Notch target gene *HRT1* (Fig. 5*F*, *upper and lower right*, respectively). These observations suggested that the altered expression of MLCK could result from a direct transcriptional effect of intracellular Notch on the *MLCK* promoter.

To test this hypothesis, we measured the sensitivity of the *MLCK* promoter to Notch signals using previously described and characterized *MLCK* promoter constructs containing sequences −6476 to +115 (p6476) or −389 to +115 (p389) driving luciferase expression (a kind gift from Dr. Paul Herring; Fig. 7*A*) (15). Co-transfection of p6476 and p389 with a myo-

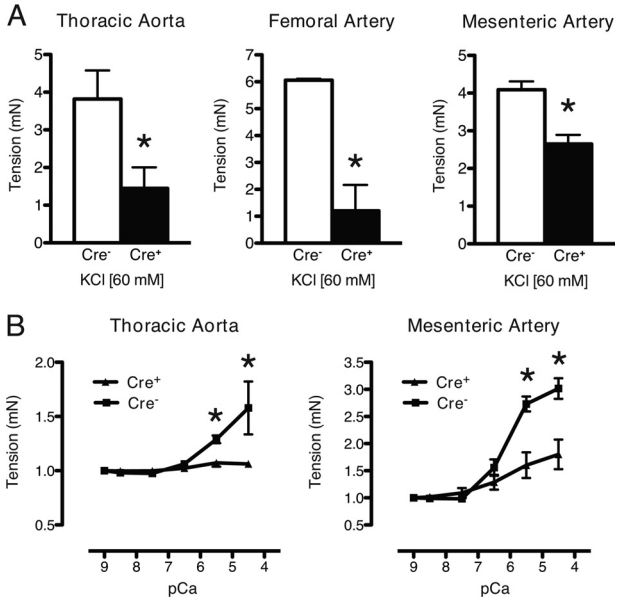

FIGURE 3. **Reduced force generation response to KCl-dependent depolarization and Ca^{2+} concentration in Notch signaling-deficient arteries.** *A*, KCl (60 mM) was added to wire-mounted arteries as indicated, resulting in impaired contractility in mutant (Cre^{+}) relative to control (Cre^{-}) vessel segments. Data are displayed as active tension relative to basal conditions in PSS buffer only. *, $p < 0.05$ *versus* control. *B*, thoracic and mesenteric arteries were permeabilized with α-toxin and exposed to incremental Ca^{2+} concentrations. For Ca^{2+}-response curves, tension was expressed as force generated above base line at *p*Ca9. Measurements were repeated in triplicate at each Ca^{2+} dose. Each data set represents mean ± S.E. (*error bars*); $n = 3$ control and 3 mutant. *, $p < 0.02$ *versus* control. *mN*, millinewtons.

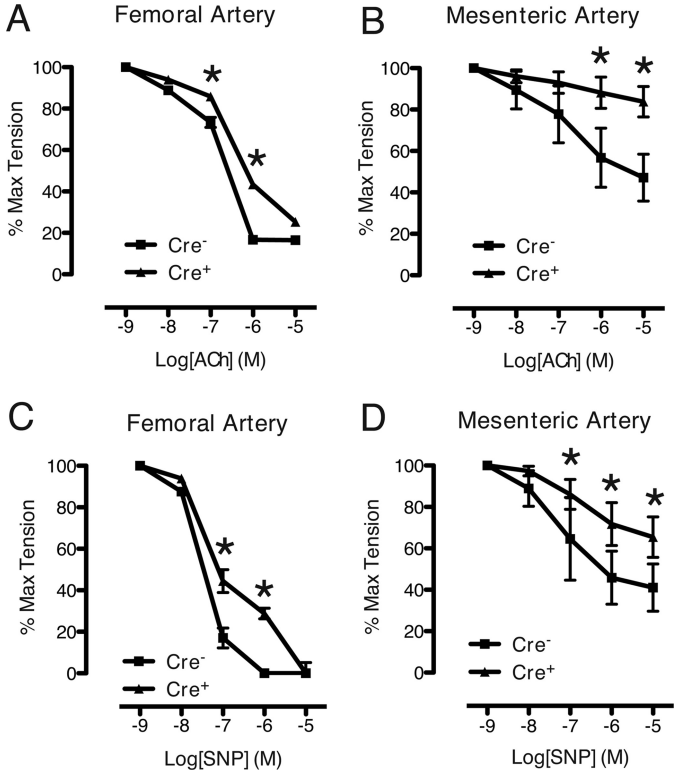

FIGURE 4. **Impaired agonist-mediated relaxation responses in Notch signaling-deficient arteries.** *A* and *B*, ACh dose-response curves from wire-mounted femoral (*A*) and mesenteric (*B*) arteries precontracted with PE. *C* and *D*, SNP dose-response curves from precontracted femoral (*C*) and mesenteric (*D*) arteries. Abnormal relaxation responses were not dependent on the endothelium. Measurements were repeated in triplicate at each agonist dose. Data are displayed as percentage of tension relative to precontracted state (100%). Each data set represents mean ± S.E. (*error bars*); $n = 3$ control and 3 mutant. *, $p < 0.05$ *versus* control.

cardin expression plasmid previously shown to enhance transcription through the CArG motif at −166 resulted in the expected increase in luciferase activity, thereby validating the functionality of these constructs (Fig. 7*B*, *Myoc*). Co-transfection of p6476 with 25 and 50 ng of constitutively active Notch1 (ICN1) expression plasmid resulted in a dose-dependent increase in luciferase activity that was abrogated by inclusion of DNMAML1 (Fig. 7*B*, *open bars*). Moreover, substitution of ICN1 with constitutively active Notch3 (ICN3) or Notch4 (ICN4) similarly enhanced luciferase activity that was abolished by DNMAML1 (supplemental Fig. 2). Importantly, although the truncated p389 promoter was reactive to myocardin, transfection with ICN1 failed to induce luciferase activity (Fig. 7*B*, *black bars*).

Thus, the sequence from −389 to −6476 is required for *MLCK* promoter response to Notch signaling. Analysis of this sequence did not reveal complete consensus CSL binding motifs as defined previously (GTGGGAA) (3, 27). However, the sequence CTGGGAA (hereafter referred to as the CC element) in which cytosine replaces the initial guanine of the consensus sequence was identified at position −3687 with 100% conservation among multiple mammalian species (UCSC Genome Browser; Fig. 7*A*). To determine whether this CC element was required for Notch activation of the *MLCK* promoter, the middle guanine was mutated to adenine on the p6476 reporter template as this is known to disrupt CSL binding (3). Two independent mutant CC clones (p2FCSL2 and p2FCSL5) containing the identical G-to-A substitution (mutant CC) were subjected to the luciferase assay. Although both clones retained expected reactivity to myocardin, ICN1 failed to activate the mutant constructs (Fig. 7*C*).

To determine whether the putative CC element at −3687 binds the Notch receptor-containing transcription complex, ChIP assays were performed with an anti-Notch1 antibody (αN1) in three different cellular contexts. First, 10T1/2 cells were co-transfected with a constitutively active ICN1 expression plasmid (pC3-ICN1) and either control vector (pGL2b), p6476, or p2FCSL2 DNAs (Fig. 7*D*). With pGL2b alone, αN1 (but not αIgG) recovered the CC element-containing DNA, suggesting a Notch1 receptor complex interaction at the endogenous *MLCK* promoter (Fig. 7*D*, *lanes 1* and *2*). Co-transfection with p6476 led to a striking enrichment of αN1-precipitated DNA containing the wild-type CC element, but no increase was observed with co-transfected p2FCSL2 DNA containing the mutated CC element (Fig. 7*D*, *lanes 4* and *6*). Second, we conducted parallel ChIP experiments in the rat A10 aortic SMC line. Again, αN1, but not αIgG, precipitated the endogenous CC element (Fig. 7*E*, *lane 2 versus lane 1*) with further enrichment from the wild-type promoter plasmid p6476 (Fig. 7*E*, *lane 4 versus lane 2*) but not from the mutated promoter in p2FCSL2 (Fig. 7*E*, *lane 6 versus lane 4*). Finally, in control SM22-Cre^{-}/$DNMAML1^{+}$ aortic SMCs propagated on prefixed Fc-Jagged1 fusion plates to further induce Notch signaling, Jagged1 stimulation resulted in enriched αN1 precipita-

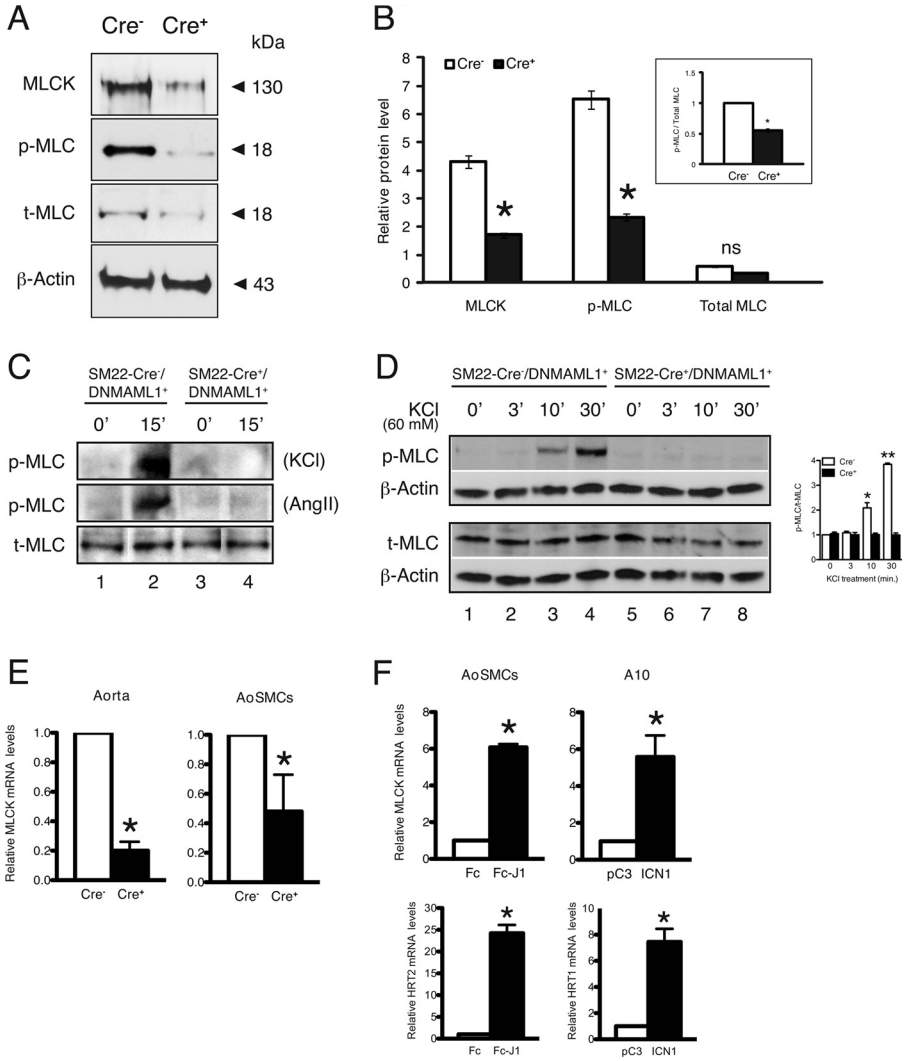

FIGURE 5. **Regulatory contractile gene expression in Notch signaling-deficient aortas and smooth muscle cells.** *A*, representative protein blots from control (SM22-Cre$^-$/DNMAML1$^+$ (*Cre*$^-$)) and mutant (SM22-Cre$^+$/DNMAML1$^+$ (*Cre*$^+$)) whole aortic extracts revealing reductions in MLCK and p-MLC content in mutants normalized to β-actin. *B*, densitometry quantitation of regulatory contractile proteins. Data are displayed as relative protein levels. The *inset box* displays the ratio of p-MLC to MLC in which densitometric units were normalized to total MLC. Data sets for protein quantitation represent mean ± S.E. (*error bars*); $n = 3$ control and 3 mutant. *, $p < 0.01$ *versus* control; *ns*, $p =$ not significant. *C*, aortic rings from mutant (SM22-Cre$^+$/DNMAML1$^+$) and littermate control (SM22-Cre$^+$/DNMAML1$^+$) animals were treated with KCl (60 mM) or Ang II (10^{-5} M) for 15 min in PSS buffer at 37 °C. Representative protein blots show induction of p-MLC relative to total (*t*)-MLC only in control rings; $n = 3$. *D*, cultured primary aortic SMCs from mutant and littermate control animals were depolarized with 60 mM KCl for the indicated duration (0–30 min). Representative protein blots from collected lysates reveal induction of p-MLC by 10 min in control (*lanes 3* and *4*) but not in corresponding Notch signaling-deficient cells (*lanes 7* and *8*). Total MLC (*t-MLC*) levels were comparable between genotypes and normalized to endogenous β-actin. Data represent $n = 3$ experimental sets. *, $p = 0.027$, **, $p < 0.001$ *versus* control. *E*, real time PCR analyses of base-line *MLCK* transcript abundance. Compared with control tissues, *MLCK* mRNA is reduced in either whole aorta (*left*) or primary aortic SMCs (*AoSMCs*) (*right*) isolated from mutant animals. *F*, real time PCR analyses of *MLCK* mRNA levels following activated Notch signaling. Jagged1 (*J1*)-induced Notch signaling in control primary aortic SMCs results in enhanced *MLCK* mRNA levels (*upper left*). The observed increase in *HRT2* transcript levels serves as a positive control for Notch activation (*lower left*). Similarly, transfected A10 rat aortic SMCs containing constitutively active ICN1 display increased *MLCK* transcripts (*upper right*) as well as an expected induction in *HRT1* expression (positive control; *lower right*). Data sets for RNA quantitation represent mean ± S.E. (*error bars*); $n = 3$ control and 3 mutant. *, $p < 0.01$ *versus* control. *Cre*$^-$, control; *Cre*$^+$, mutant.

tion of the conserved CC element in the endogenous *MLCK* promoter (Fig. 7*F*, *lane 4 versus lane 2*). Taken together, these findings identify a novel Notch signaling-sensitive element in the *MLCK* promoter, providing a molecular mechanism through which Notch signaling regulates VSM contractile function.

DISCUSSION

The SM22-Cre$^+$/DNMAML1$^+$ model of pan-Notch receptor inhibition in VSM demonstrates a novel role for Notch signaling in the transcriptional control of systemic arterial VSM function. Prior studies in a murine model of CADASIL syndrome demonstrated altered responses of cerebral and caudal arteries to mechanical (flow and pressure) but not agonist-induced reactivity (10, 28). Additional examination of Notch3-deficient mice revealed functional perturbations limited to cerebral blood flow autoregulation and vascular tone in tail arteries but not to other arteries, including carotid, pulmonary, and aorta (7, 8, 11, 29). Despite failed mechanotransduction of tensile stress, responses to agonist or Ca^{2+} stimulation were preserved in cerebral and tail arteries (8, 29). Aortic and pulmonary arteries from Notch3-deficient mice displayed normal

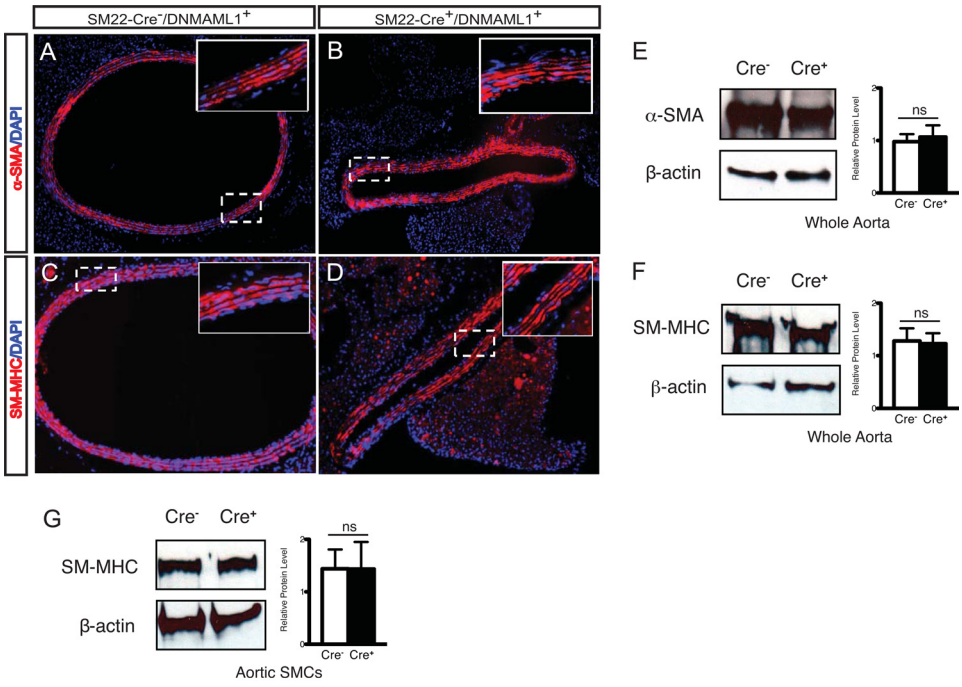

FIGURE 6. **VSM contractile protein expression patterns in Notch signaling-deficient thoracic aorta.** Transverse sections display immunoreactivities for α-SMA (*A* and *B*) and SM-MHC (*C* and *D*) in aorta from control (*Cre*$^-$) and SM22-Cre$^+$/DNMAML1$^+$ (*Cre*$^+$) mice. α-SMA and SM-MHC expression in the tunica media was similar between groups. *Boxed insets* in *A–D* display high magnification of the tunica media. Nuclei are counterstained with DAPI (*blue*). Representative protein blot and densitometry quantitation of α-SMA (*E*) and SM-MHC (*F*) relative to endogenous β-actin levels from control and SM22-Cre$^+$/DNMAML1$^+$ whole aortas are shown. Data display mean ± S.E. (*error bars*); $n = 3$. *ns*, p = not significant. Representative protein blot and densitometry quantitation of SM-MHC relative to endogenous β-actin levels from control and SM22-Cre$^+$/DNMAML1$^+$ primary aortic SMCs (*G*) are shown. Data display mean ± S.E. (*error bars*); $n = 3$. *ns*, p = not significant.

responses to depolarization and agonist-mediated vasoconstriction (7, 11). More recently, re-examination of Notch3-deficient mice has uncovered a blood flow-dependent autoregulatory defect in renal afferent arterioles; however, non-renal arterioles from these animals functioned comparably with controls (9). Interestingly, in those study animals, blood pressure was acutely sensitive to high doses of Ang II but not norepinephrine; however, the basis for this differential response was not clear. Hence, several mouse models of Notch3 signaling dysregulation have exposed roles for this receptor primarily in transducing mechanostimulation within a subset of arteries, but the molecular mechanism underlying this specificity remains unclear.

An important feature of the aforementioned genetic models is the presence of other Notch receptors in VSM along with unaltered expression of Notch target gene families *HEY* and *HES* (29). In one study, reductions in HEY1 and HES1 appeared limited to cerebral but not aortic SMCs from Notch3-deficient mice (7). Therefore, Notch signaling in VSM may not be fully suppressed in these models. By abrogating canonical Notch signaling through elaboration of DNMAML1 in VSM, our studies demonstrate a substantially broader role for Notch signaling in regulating the function of systemic arteries. Our data suggest that either the sum total of Notch signaling output and/or combined signaling through Notch receptors (in addition to Notch3) influences the molecular and functional status of VSM by compromising select component(s) of the contractile apparatus.

Importantly, force generation of Notch signaling-deficient arterial segments was reduced in response to multiple triggers, including agonists, depolarization, and calcium. The markedly diminished calcium sensitivity of force production in permeabilized preparations is consistent with decreases in MLCK and its activity as indicated by reduced levels of p-MLC. Lack of force production and p-MLC could also result from increased expression or activity of MP, but in fact, MP expression was surprisingly reduced in mutant aorta (data not shown). That MP activity may be reduced in this model is suggested by the blunted response to vasorelaxants. However, constrictor, dilator, and depolarization responses require many genes acting through numerous signaling pathways ultimately converging on the activities of MLCK and MP. These measured observations in the mutant vessels and animals might reflect a re-established hemodynamic equilibrium triggered by altered MLCK and exemplified by similar base-line blood pressures between cohorts. Further investigation will be necessary to address additional interactions and linkage between Notch signals and MLCK and MP regulation.

Interestingly, we did not identify altered levels of VSM differentiation markers SM-MHC and αSMA in mutant aortas, suggesting a selective influence by Notch signaling on the contractile apparatus in this animal model. *In vitro* studies have shown that Notch signals can promote the transcriptional activity of these contractile genes through CSL recognition motifs in their promoters, an effect possibly dependent on serum response factor/myocardin (30, 31). In contrast, forced expression of constitutively active Notch1 (ICN1) or HRT proteins inhibited myocardin-mediated activation of SM-MHC and αSMA in smooth muscle differentiation systems (26, 32). Therefore, our finding of unaltered myofilament levels and his-

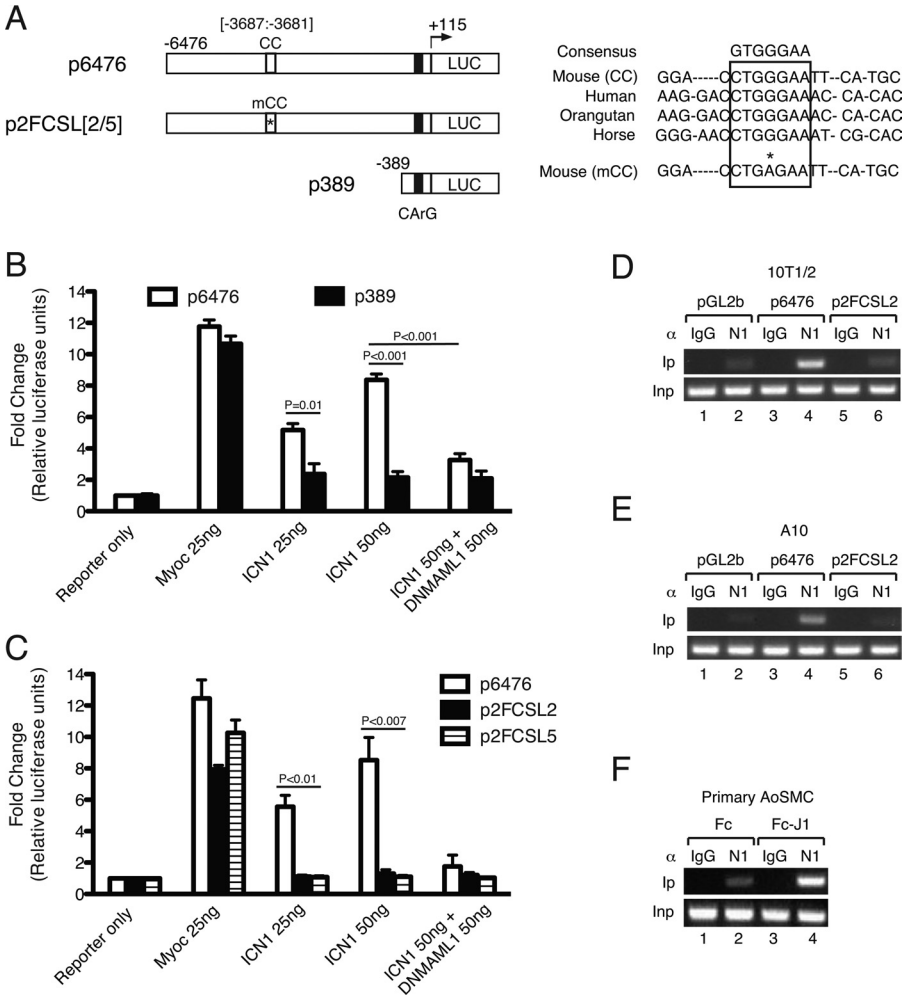

FIGURE 7. ***MLCK* promoter is transduced by canonical Notch signaling.** *A*, schematic representation of long (p6476) and short (p389) *MLCK* promoter-luciferase (*LUC*) constructs and modified constructs p2FCSL2 and p2FCSL5 containing a mutated core CSL element. The *right panel* displays mammalian sequence homologies at the *MLCK* promoter region containing the core CSL element at −3687. The *asterisk* denotes G-to-A substitution within the core CSL element. *CC*, core CSL element; *mCC*, mutant core CSL element; CArG *box*, serum response factor-binding element. *B* and *C*, luciferase assay in transfected 10T1/2 cells. *B*, incremental (25 and 50 ng of plasmid) ICN1 expression transactivates p6476 (*open bars*) but not p389 (*solid bars*). Inclusion of DNMAML1 expression abrogates ICN1 induction (50 ng of ICN1 + 50 ng of DNMAML1). The data set represents mean ± S.E. (*error bars*); $n = 3$. *C*, compared with unmodified p6475 (*open bars*), p2FCSL2/5 constructs (*solid* and *hatched bars*) were not transduced by ICN1 but retained sensitivity to myocardin (*Myoc*) (see text). The data set represents mean ± S.E. (*error bars*); $n = 3$. *D–F*, chromatin immunoprecipitation using anti-Notch1 antibody (αN1) *versus* control (αIgG) suggests enrichment of Notch1 complex within the *MLCK* promoter region containing the CC element at −3687. αN1 precipitation in 10T1/2 (*D*) or A10 (*E*) cells following transfection with a constitutively active ICN1 expression plasmid and either pGL2b (control vector), p6476, or p2FCSL2 DNAs. Enriched precipitation by αN1 of promoter sequence containing the CC element occurs in p6476-transfected cells (*D* and *E*, *lane 4*) but not in p2FCSL2-containing cells (*D* and *E*, *lane 6*) showing only endogenous *MLCK* promoter precipitation (*D* and *E*, *pGL2b*, *lane 2*). *F*, primary Cre^- aortic SMCs (*AoSMCs*)were propagated on culture dishes displaying fixed Jagged1 ligand (Fc-Jagged1 fusion (*Fc-J1*)) or control (*Fc*). Compared with Fc only (*lane 2*), Fc-Jagged1 fusion-stimulated SMCs demonstrated enhanced αN1 complex precipitation of the endogenous *MLCK* promoter containing the conserved CC sequence (*lane 4*). α, antibody; *Ip*, immunoprecipitate; *Inp*, input DNA. ChIP data sets are representative of $n = 3$ experiments per cell type.

tologically normal tunica media in Notch signaling-deficient TA vessels may seem surprising but likely reflects a dominant role for myocardin in governing SM-MHC and αSMA expression *in vivo*. Our current studies of the *MLCK* promoter suggest that its activation by myocardin does not require the Notch-sensitive CC element, but it remains to be determined whether synergism with Notch signaling activation or inhibition is a regulatory feature of *MLCK* gene expression.

Unlike the characteristic thin walled and dilated cerebral arteries described previously in $SM22\text{-}Cre^+/DNMAML1^+$ mice, we did not observe similar abnormalities in aortic wall structure that might explain force generation deficits. Such morphometric differences possibly reflect regional functionality and intrinsic compensatory signals in VSM derived from different developmental lineages. In a preliminary ultrastructural examination of the aorta, subtle increases in intercellular space within the tunica media were apparent, but the significance of this finding remains uncertain (data not shown). For example, cerebral arteries from Notch3-deficient mice feature thin tunica media, and tail arteries display non-cohesive VSM cells associated with poor pressure-induced myogenic responses but intact agonist reactivity (8, 29). In contrast, Arboleda-Velasquez *et al.* (7) examined a Notch3-deficient murine model that did not yield morphological abnormalities in brain vessels or aorta. Functional studies using their model identified a susceptibility to induced stroke associated with cerebral blood flow abnormalities and a transcriptome array of down-regulated contractile genes (including *MLCK*) specifically in brain

but not aortic VSM cells (7). Finally, VSM in transgenic CADASIL mice featured cytoskeletal abnormalities and disruption of intercellular adhesion associated with defective pressure-induced mechanostimulation but preserved agonist-induced contractility (33). These examples illustrate that abnormal VSM intercellular contacts resulting from altered Notch3 signaling can be associated with impaired myogenic responses but normal agonist- or depolarization-induced force generation.

Similar findings of selective contractile impairment derive from murine models wherein the absence of cytoskeletal vimentin or dystrophin protein impairs arterial mechanotransduction but not agonist-triggered responses, and in vimentin-deficient airway smooth muscle, defective contractility is not associated with impaired MLCK activity (34–36). Finally, studies using specific gap junction inhibitors reported a key role for cell adhesion in myogenic responses but not agonist-induced vasoconstriction, whereas other inhibitors abolished vasoconstrictor responses but preserved depolarization-induced reactivity (37–39). Together, these studies highlight the complex relationships that exist among VSM cell adhesion, cytoskeletal filaments, and signals regulating MLC phosphorylation and myosin activity.

In conclusion, we find that canonical Notch signaling through the transcriptional control of key regulatory contractile proteins is required for the contractile function of mature arterial VSM. However, our data do not exclude the existence of additional transcription-independent mechanisms through which Notch might regulate MLCK, and such possibilities will require further exploration. It is noteworthy that the clinical efficacy of γ-secretase inhibition (pan-Notch receptor inhibition) for treatment of diverse diseases, including select malignancies and Alzheimer dementia, is under active investigation (40–42). Our current study suggests that such therapies could impact vascular function if sufficient inhibition of Notch signaling occurs within the VSM compartment. Alternatively, pharmacological or genetic manipulation of VSM Notch signaling may be a useful and novel strategy for modulating arterial reactivity.

Acknowledgments—We thank Praveen N. Pakeerappa and Dr. Ian Bratz for technical assistance with arterial myography and surgical procedures and are grateful to Dr. Paul Herring for the gift of MLCK promoter-reporter constructs.

REFERENCES

1. Mumm, J. S., and Kopan, R. (2000) Notch signaling: from the outside in. *Dev. Biol.* **228,** 151–165
2. Nam, Y., Sliz, P., Song, L., Aster, J. C., and Blacklow, S. C. (2006) Structural basis for cooperativity in recruitment of MAML coactivators to Notch transcription complexes. *Cell* **124,** 973–983
3. Tun, T., Hamaguchi, Y., Matsunami, N., Furukawa, T., Honjo, T., and Kawaichi, M. (1994) Recognition sequence of a highly conserved DNA binding protein RBP-Jκ. *Nucleic Acids Res.* **22,** 965–971
4. Fischer, A., Schumacher, N., Maier, M., Sendtner, M., and Gessler, M. (2004) The Notch target genes Hey1 and Hey2 are required for embryonic vascular development. *Genes Dev.* **18,** 901–911
5. Sakata, Y., Xiang, F., Chen, Z., Kiriyama, Y., Kamei, C. N., Simon, D. I., and Chin, M. T. (2004) Transcription factor CHF1/Hey2 regulates neointimal formation in vivo and vascular smooth muscle proliferation and migration *in vitro*. *Arterioscler. Thromb. Vasc. Biol.* **24,** 2069–2074
6. Chabriat, H., Joutel, A., Dichgans, M., Tournier-Lasserve, E., and Bousser, M. G. (2009) Cadasil. *Lancet Neurol.* **8,** 643–653
7. Arboleda-Velasquez, J. F., Zhou, Z., Shin, H. K., Louvi, A., Kim, H. H., Savitz, S. I., Liao, J. K., Salomone, S., Ayata, C., Moskowitz, M. A., and Artavanis-Tsakonas, S. (2008) Linking Notch signaling to ischemic stroke. *Proc. Natl. Acad. Sci. U.S.A.* **105,** 4856–4861
8. Belin de Chantemèle, E. J., Retailleau, K., Pinaud, F., Vessières, E., Bocquet, A., Guihot, A. L., Lemaire, B., Domenga, V., Baufreton, C., Loufrani, L., Joutel, A., and Henrion, D. (2008) Notch3 is a major regulator of vascular tone in cerebral and tail resistance arteries. *Arterioscler. Thromb. Vasc. Biol.* **28,** 2216–2224
9. Boulos, N., Helle, F., Dussaule, J. C., Placier, S., Milliez, P., Djudjaj, S., Guerrot, D., Joutel, A., Ronco, P., Boffa, J. J., and Chatziantoniou, C. (2011) Notch3 is essential for regulation of the renal vascular tone. *Hypertension* **57,** 1176–1182
10. Dubroca, C., Lacombe, P., Domenga, V., Maciazek, J., Levy, B., Tournier-Lasserve, E., Joutel, A., and Henrion, D. (2005) Impaired vascular mechanotransduction in a transgenic mouse model of CADASIL arteriopathy. *Stroke* **36,** 113–117
11. Li, X., Zhang, X., Leathers, R., Makino, A., Huang, C., Parsa, P., Macias, J., Yuan, J. X., Jamieson, S. W., and Thistlethwaite, P. A. (2009) Notch3 signaling promotes the development of pulmonary arterial hypertension. *Nat. Med.* **15,** 1289–1297
12. He, W. Q., Qiao, Y. N., Zhang, C. H., Peng, Y. J., Chen, C., Wang, P., Gao, Y. Q., Chen, C., Chen, X., Tao, T., Su, X. H., Li, C. J., Kamm, K. E., Stull, J. T., and Zhu, M. S. (2011) Role of myosin light chain kinase in regulation of basal blood pressure and maintenance of salt-induced hypertension. *Am. J. Physiol. Heart Circ. Physiol.* **301,** H584–H591
13. Ito, M., Nakano, T., Erdodi, F., and Hartshorne, D. J. (2004) Myosin phosphatase: structure, regulation and function. *Mol. Cell. Biochem.* **259,** 197–209
14. Herring, B. P., El-Mounayri, O., Gallagher, P. J., Yin, F., and Zhou, J. (2006) Regulation of myosin light chain kinase and telokin expression in smooth muscle tissues. *Am. J. Physiol. Cell Physiol.* **291,** C817–C827
15. Yin, F., Hoggatt, A. M., Zhou, J., and Herring, B. P. (2006) 130-kDa smooth muscle myosin light chain kinase is transcribed from a CArG-dependent, internal promoter within the mouse mylk gene. *Am. J. Physiol. Cell Physiol.* **290,** C1599–C1609
16. Kamm, K. E., and Stull, J. T. (2001) Dedicated myosin light chain kinases with diverse cellular functions. *J. Biol. Chem.* **276,** 4527–4530
17. Somlyo, A. P., and Somlyo, A. V. (2003) Ca^{2+} sensitivity of smooth muscle and nonmuscle myosin II: modulated by G proteins, kinases, and myosin phosphatase. *Physiol. Rev.* **83,** 1325–1358
18. Proweller, A., Wright, A. C., Horng, D., Cheng, L., Lu, M. M., Lepore, J. J., Pear, W. S., and Parmacek, M. S. (2007) Notch signaling in vascular smooth muscle cells is required to pattern the cerebral vasculature. *Proc. Natl. Acad. Sci. U.S.A.* **104,** 16275–16280
19. Zhang, H., and Fisher, S. A. (2007) Conditioning effect of blood flow on resistance artery smooth muscle myosin phosphatase. *Circ. Res.* **100,** 730–737
20. Mulvany, M. J., and Halpern, W. (1977) Contractile properties of small arterial resistance vessels in spontaneously hypertensive and normotensive rats. *Circ. Res.* **41,** 19–26
21. Lu, Y., Zhang, H., Gokina, N., Mandala, M., Sato, O., Ikebe, M., Osol, G., and Fisher, S. A. (2008) Uterine artery myosin phosphatase isoform switching and increased sensitivity to SNP in a rat L-NAME model of hypertension of pregnancy. *Am. J. Physiol. Cell Physiol.* **294,** C564–C571
22. Yang, K., and Proweller, A. (2011) Vascular smooth muscle Notch signals regulate endothelial cell sensitivity to angiogenic stimulation. *J. Biol. Chem.* **286,** 13741–13753
23. Khatri, J. J., Joyce, K. M., Brozovich, F. V., and Fisher, S. A. (2001) Role of myosin phosphatase isoforms in cGMP-mediated smooth muscle relaxation. *J. Biol. Chem.* **276,** 37250–37257
24. Satterwhite, L. L., Lohka, M. J., Wilson, K. L., Scherson, T. Y., Cisek, L. J., Corden, J. L., and Pollard, T. D. (1992) Phosphorylation of myosin-II regulatory light chain by cyclin-p34cdc2: a mechanism for the timing of cytokinesis. *J. Cell Biol.* **118,** 595–605

25. Zhi, G., Ryder, J. W., Huang, J., Ding, P., Chen, Y., Zhao, Y., Kamm, K. E., and Stull, J. T. (2005) Myosin light chain kinase and myosin phosphorylation effect frequency-dependent potentiation of skeletal muscle contraction. *Proc. Natl. Acad. Sci. U.S.A.* **102,** 17519–17524
26. Proweller, A., Pear, W. S., and Parmacek, M. S. (2005) Notch signaling represses myocardin-induced smooth muscle cell differentiation. *J. Biol. Chem.* **280,** 8994–9004
27. Del Bianco, C., Vedenko, A., Choi, S. H., Berger, M. F., Shokri, L., Bulyk, M. L., and Blacklow, S. C. (2010) Notch and MAML-1 complexation do not detectably alter the DNA binding specificity of the transcription factor CSL. *PLoS One* **5,** e15034
28. Lacombe, P., Oligo, C., Domenga, V., Tournier-Lasserve, E., and Joutel, A. (2005) Impaired cerebral vasoreactivity in a transgenic mouse model of cerebral autosomal dominant arteriopathy with subcortical infarcts and leukoencephalopathy arteriopathy. *Stroke* **36,** 1053–1058
29. Domenga, V., Fardoux, P., Lacombe, P., Monet, M., Maciazek, J., Krebs, L. T., Klonjkowski, B., Berrou, E., Mericskay, M., Li, Z., Tournier-Lasserve, E., Gridley, T., and Joutel, A. (2004) Notch3 is required for arterial identity and maturation of vascular smooth muscle cells. *Genes Dev.* **18,** 2730–2735
30. Doi, H., Iso, T., Sato, H., Yamazaki, M., Matsui, H., Tanaka, T., Manabe, I., Arai, M., Nagai, R., and Kurabayashi, M. (2006) Jagged1-selective notch signaling induces smooth muscle differentiation via a RBP-Jκ-dependent pathway. *J. Biol. Chem.* **281,** 28555–28564
31. Noseda, M., Fu, Y., Niessen, K., Wong, F., Chang, L., McLean, G., and Karsan, A. (2006) Smooth muscle α-actin is a direct target of Notch/CSL. *Circ. Res.* **98,** 1468–1470
32. Doi, H., Iso, T., Yamazaki, M., Akiyama, H., Kanai, H., Sato, H., Kawai-Kowase, K., Tanaka, T., Maeno, T., Okamoto, E., Arai, M., Kedes, L., and Kurabayashi, M. (2005) HERP1 inhibits myocardin-induced vascular smooth muscle cell differentiation by interfering with SRF binding to CArG box. *Arterioscler. Thromb. Vasc. Biol.* **25,** 2328–2334
33. Ruchoux, M. M., Domenga, V., Brulin, P., Maciazek, J., Limol, S., Tournier-Lasserve, E., and Joutel, A. (2003) Transgenic mice expressing mutant Notch3 develop vascular alterations characteristic of cerebral autosomal dominant arteriopathy with subcortical infarcts and leukoencephalopathy. *Am. J. Pathol.* **162,** 329–342
34. Henrion, D., Terzi, F., Matrougui, K., Duriez, M., Boulanger, C. M., Colucci-Guyon, E., Babinet, C., Briand, P., Friedlander, G., Poitevin, P., and Lévy, B. I. (1997) Impaired flow-induced dilation in mesenteric resistance arteries from mice lacking vimentin. *J. Clin. Investig.* **100,** 2909–2914
35. Loufrani, L., Matrougui, K., Gorny, D., Duriez, M., Blanc, I., Lévy, B. I., and Henrion, D. (2001) Flow (shear stress)-induced endothelium-dependent dilation is altered in mice lacking the gene encoding for dystrophin. *Circulation* **103,** 864–870
36. Wang, R., Li, Q., and Tang, D. D. (2006) Role of vimentin in smooth muscle force development. *Am. J. Physiol. Cell Physiol.* **291,** C483–C489
37. Christ, G. J., Spektor, M., Brink, P. R., and Barr, L. (1999) Further evidence for the selective disruption of intercellular communication by heptanol. *Am. J. Physiol. Heart Circ. Physiol.* **276,** H1911–H1917
38. Earley, S., Resta, T. C., and Walker, B. R. (2004) Disruption of smooth muscle gap junctions attenuates myogenic vasoconstriction of mesenteric resistance arteries. *Am. J. Physiol. Heart Circ. Physiol.* **287,** H2677–H2686
39. Lagaud, G., Gaudreault, N., Moore, E. D., Van Breemen, C., and Laher, I. (2002) Pressure-dependent myogenic constriction of cerebral arteries occurs independently of voltage-dependent activation. *Am. J. Physiol. Heart Circ. Physiol.* **283,** H2187–H2195
40. Aster, J. C., Blacklow, S. C., and Pear, W. S. (2011) Notch signalling in T-cell lymphoblastic leukaemia/lymphoma and other haematological malignancies. *J. Pathol.* **223,** 262–273
41. Wang, Z., Li, Y., Banerjee, S., and Sarkar, F. H. (2008) Exploitation of the Notch signaling pathway as a novel target for cancer therapy. *Anticancer Res.* **28,** 3621–3630
42. Wolfe, M. S. (2008) Inhibition and modulation of γ-secretase for Alzheimer's disease. *Neurotherapeutics* **5,** 391–398